Accepted for Publication in The Astrophysical Journal
Preprint typeset using LaTeX style emulateapj v. 6/22/04

arXiv:astro-ph/0505415v1 19 May 2005

THE HEATED CORE OF THE RADIO-QUIET GALAXY CLUSTER A644

David A. Buote[1], Philip J. Humphrey[1], & John T. Stocke[2]

Accepted for Publication in The Astrophysical Journal

ABSTRACT

We present an analysis of a *Chandra* ACIS-I observation of the massive galaxy cluster A644. This cluster was previously classified as a cooling flow, but no radio emission has been detected from its cD galaxy. Outside the core ($R \sim 75$ kpc $\sim 0.03 r_{\rm vir}$) the hot ICM has properties consistent with a (relaxed) cool-core cluster out to the largest radii investigated ($R \sim 415$ kpc $\sim 0.14 r_{\rm vir}$). Over this region the gravitating mass profile is described well by a Navarro-Frenk-White profile with concentration parameter, $c = 6.1 \pm 1.2$, and virial radius, $r_{\rm vir} = 2.9 \pm 0.4$ Mpc. However, inside the core the temperature and entropy profiles reverse their inward radial decline and rise at the center; the inner temperature profile is inconsistent with a constant at the 2.3σ level. Although the core region does not display X-ray cavities or filamentary structures characteristic of radio-loud, cool-core clusters, the peak of the X-ray emission is offset from that of the centroid of the global X-ray halo by ≈ 60 kpc. The position of the cD galaxy lies approximately between the X-ray peak and centroid, further testifying to a merger origin for the properties of the X-ray emission in the core. We discuss the implications of A644 and the small number of radio-quiet, cool-core clusters for the AGN feedback paradigm to suppress cooling flows in clusters.

Subject headings: X-rays: galaxies: clusters – galaxies: halos – galaxies: formation – cooling flows – galaxies: clusters: individual: A644

1. INTRODUCTION

XMM and *Chandra* grating and CCD observations of the cores of clusters previously believed to be harboring cooling flows find very little gas cooling below $T \sim 1$ keV (e.g., Peterson et al. 2001, 2003; Tamura et al. 2001; David et al. 2001; Molendi & Pizzolato 2001; Xu et al. 2002; Ettori et al. 2002; Buote et al. 2003a). This major discovery has led to the widely discussed picture where feedback on the hot intracluster medium (ICM) from an AGN in the central cluster galaxy is responsible for stifling the cooling flow, though the details of the heating process remain elusive (e.g., for reviews see Mathews & Brighenti 2003; Fabian 2004). About 70% of clusters previously classified as cooling flows possess radio emission from the central galaxy (e.g., Burns 1990). *Chandra* observations indicate that such clusters also have X-ray cavities and filamentary structures in the X-ray images that are related to the radio emission (e.g., Fabian et al. 2000; McNamara et al. 2000; Blanton et al. 2001; Mazzotta et al. 2003; Bîrzan et al. 2004).

What about clusters indicated to be cooling flows from previous low-resolution X-ray observations that do not display radio properties typical of cooling flows? We have previously analyzed *Chandra* observations of two such systems: A2029 (Lewis et al. 2002, 2003) and A2589 (Buote & Lewis 2004). A2589 has no observed radio emission associated with its cD galaxy; and, although the cD in A2029 does possess a Wide-Angle-Tail (WAT) radio source, such sources are generally not found in cooling flows (Owen et al. 1984; Burns 1990), though their morphology provides evidence for relative motions between the radio source and ICM (Eilek et al. 1984; Burns et al. 2002). Both of these clusters have high density cores with temperatures significantly lower than at larger radii. (Although the relatively low-quality *Chandra* data of A2589 are consistent with an isothermal gas, a new *XMM* observation clearly indicates that the temperature profile increases with radius – Zappacosta et al. 2005, in preparation.) These clusters also display no spectroscopic evidence for cooling flows and have unusually symmetric X-ray images without the pronounced surface brightness irregularities observed in the cores of "radio loud" cool-core clusters (e.g., Bîrzan et al. 2004). Finally, cool-core clusters also appear to preferentially display central metallicity enhancements, while flat metallicity profiles are characteristic of non-cooling flow, generally disturbed, systems (e.g., De Grandi et al. 2004; Böhringer et al. 2004). A2589 and A2029 both have pronounced central metallicity enhancements further attesting to their comparatively relaxed states.

Observations suggest that cooling flows are destroyed by large turbulent motions in the ICM since major merging activity in clusters anti-correlates with cooling mass-flow rate (Buote & Tsai 1996), a conclusion supported by theoretical studies (e.g., Roettiger et al. 1996; Norman & Bryan 1999; Fujita et al. 2004). Likewise, theoretical studies (e.g., Loken et al. 1995; Roettiger et al. 1996) suggest that WAT radio morphology may also be a signature of hot shocks in on-going cluster mergers. Since the X-ray images of A2029 and A2589 are very regular all the way into their cores (though see §6), and yet there is no evidence for ICM cooling or radio emission typical of cool-core clusters, in the context of the AGN feedback paradigm we are viewing these clusters at a special time after they have settled down from past mergers but very soon before the onset of AGN heating.

Here we examine a *Chandra* observation of A644, an-

[1] Department of Physics and Astronomy, University of California at Irvine, 4129 Frederick Reines Hall, Irvine, CA 92697-4575
[2] Center for Astrophysics and Space Astronomy, University of Colorado, 389 UCB, Boulder, CO 80309

other "radio quiet" cluster that was previously classified as a cooling flow based on analysis of both X-ray imaging and spectral data (Edge et al. 1992; Peres et al. 1998). A644 is the only cooling flow cluster with large inferred $\dot{M}$ ($> 100\ M_\odot\ \mathrm{yr}^{-1}$), which was not detected in the radio study of Burns (1990, $P_{6\mathrm{cm}} < 3\ \mathrm{x}10^{21}$ W Hz^{-1}). We wish to examine how its X-ray properties compare to the other cooling flow clusters with atypical radio properties and, in particular, whether it demonstrates a clearer connection between past merger activity and the suppression of a cooling flow. The redshift of A644 ($z = 0.0704$) corresponds to an angular diameter distance of 277 Mpc and $1'' = 1.34$ kpc assuming $\Omega_\mathrm{m} = 0.3$, $\Omega_\Lambda = 0.7$, and $H_0 = 70$ km s^{-1} Mpc^{-1}.

The paper is organized as follows. In §2 we present the observation and discuss the data reduction. The analysis of the image and spectral data of the ACIS-I are presented in §3 and §4 respectively. We calculate the gravitating matter distribution in §5. Finally, in §6 we present our conclusions.

2. OBSERVATIONS AND DATA ANALYSIS

A644 was observed with the ACIS-I CCD array for approximately 30 ks during AO-2 as part of the *Chandra* Guest Observer program. We reduced the data using the CIAO v3.1 (with CALDB v2.28) and HEASOFT v5.3.1 software packages. We followed the standard CIAO threads[3] and reprocessed the level-1 events data to make use of the latest calibration information, including correcting for charge-transfer inefficiency and a time-dependent gain shift. From regions of least source contamination of the CCDs we extracted a light-curve (5.0-10.0 keV) to identify periods of high background. The observation was remarkably quiescent, and after removing a small period of modestly increased background rate, the total exposure used for subsequent analysis was 28.9 ks.

Since the cluster emission fills the entire ACIS-I field, we adopted for our default analysis the standard background events files provided in the CALDB collected from suitable blank fields. For comparison to results obtained using these standard background templates, we also modeled the background directly. Using regions as far away from the cluster center as possible, we extracted a spectrum (with point sources masked out) and fitted it with a combined source and background model (e.g., Buote et al. 2004). For the source, we adopted a thin thermal plasma component (APEC) with $T = 6$ keV and half-solar metallicity. The background was modeled with components for the Cosmic X-ray Background (CXB) and instrumental background: two soft APEC thermal plasmas and a hard power law for the CXB; a broken power law and two gaussians for the instrumental background. Comparison of results using the alternative background is presented in §4.

3. IMAGING ANALYSIS

In Figure 1 we display the ACIS-I image of A644 in the 0.3-7.0 keV band. The image was corrected for exposure variations using an exposure map created for a monochromatic energy 1 keV, approximately the counts-weighted average energy of the spectrum. For presentation purposes only, the image was also adaptively smoothed using the CIAO task CSMOOTH with default parameter settings. The diffuse emission is seen to fill the entire ACIS-I field. The morphology of most of the cluster is quite regular and approximately elliptical in shape.

Visual inspection of the central $R \sim 30''$ region of the (smoothed) X-ray surface brightness reveals some irregular, non-azimuthally symmetric features (Figure 1). These deviations from a symmetric configuration, though statistically significant, do not represent large fluctuations ($< 10\%$) in the mean surface brightness level. In particular, the data do not provide clear evidence for distinct subclumps in the core region.

We also searched for azimuthal fluctuations in the core by constructing a hardness ratio map (and also through spectral fitting in sectors, see §4). We did not find any corresponding azimuthal fluctuations either in the core or on larger scales. Instead, we found the spectrally softer core gives way at larger radius to a spectrally harder surrounding medium. This radial variation is consistent with the radially increasing temperature profile (see §4).

We measure the centroid and the ellipticity of the X-ray surface brightness using the moment method described by Carter & Metcalfe (1980) and implemented in our previous X-ray studies of galaxies and clusters (e.g., Buote & Canizares 1994). This iterative method is equivalent to computing the (two-dimensional) principal moments of inertia within an elliptical region. The ellipticity is defined by the square root of the ratio of the principal moments, and the position angle is defined by the orientation of the larger principal moment. Following our previous study of the ellipticity of the *Chandra* data of NGC 720 (Buote et al. 2002) we removed point sources and replaced them with smoothly distributed diffuse emission using the CIAO task DMFILTH.

The centroid of the X-ray surface brightness shifts significantly (e.g., $\Delta R = 56 \pm 6$ kpc between 15-500 kpc), mostly directed toward the South. At the smallest radii the centroid is located within the region of image irregularities in the core mentioned above. Outside of the core region the X-ray isophotes are very regular and moderately elliptical. The ellipticity gently falls from 0.30 ± 0.02 at $a = 100$ kpc to 0.243 ± 0.004 at $a = 500$ kpc, where a is the semi-major axis of the elliptical aperture within which the moments are calculated. Over this radius range the position angle (measured N through E) of the elliptical apertures is quite steady, varying between a maximum of 11 ± 2 degrees (at $a = 100$ kpc) and a minimum of 6 ± 0.5 degrees (at $a = 300$ kpc). Overall, the image properties suggest a relaxed cluster outside about $R \approx 100$ kpc but a disturbed cluster within $R \approx 50$ kpc.

We examined the radial surface brightness profile (with point sources masked out) located about the X-ray peak and also about the centroid computed within $a = 500$ kpc. In both cases the surface brightness profile is fitted fairly well out to $R = 600$ kpc by a β model: $r_c = 79 \pm 2$ kpc, $\beta = 0.50 \pm 0.01$, $\chi^2 = 200.4$, 129 dof (peak) and $r_c = 118 \pm 3$ kpc, $\beta = 0.59 \pm 0.01$, $\chi^2 = 198.6$, 128 dof (centroid). The largest fit residuals ($\sim 20\%$) lie within the innermost region ($r \lesssim 10''$) and are modest ($< 5\%$) elsewhere. We note that the parameters r_c and β increase systematically when we include data from increasingly larger radii or exclude data from the

[3] http://asc.harvard.edu/ciao/threads

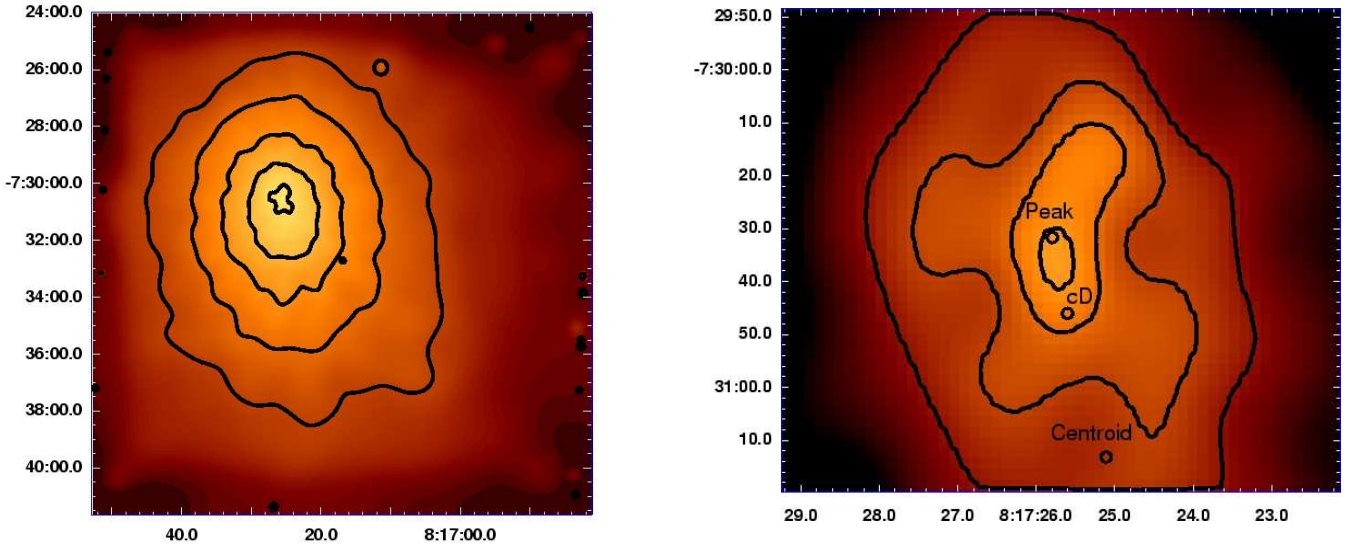

FIG. 1.— (*Left*) Smoothed, exposure-corrected ACIS-I image of A644 in the 0.3-7.0 keV band before point sources have been removed. Overlaid contours are logarithmically spaced in intensity. (*Right*) Close-up of the $R \approx 45''$ region centered about the emission peak. The small circles indicate the (J2000) positions of the peak (08h17m25.793s,-07d30m31.69s) and centroid (08h17m25.106s,-07d31m13.14s) determined from the X-ray data and the optical position of the cD galaxy (08h17m25.6s,-07d30m46s). Note that the peak is computed by centroiding on the 30 brightest pixels.

very central region. Both of these issues likely account for the different values obtained from previous *ROSAT* studies which included data at larger radii; e.g., using the PSPC Ettori & Fabian (1999) obtain $r_c = 157$ kpc and $\beta = 0.69$.

4. SPECTRAL ANALYSIS

We focus our attention on the spectral properties of the hot gas obtained within a series of concentric circular annuli centered either on the X-ray centroid or peak. Below we also briefly discuss attempts to constrain azimuthal variations in the spectral properties. The widths of the circular annuli were chosen so that the temperatures were determined to similar precision in each radial bin. For the centroid case we list the annuli in Table 1. Annuli 1-4 contain 10^4 background-subtracted counts while bins 5-9 contain twice that amount in the 1.5-7 keV band. We restrict our analysis to energies above 1.5 keV because of uncertainties arising from excess absorption above the Galactic value discussed below, and because the gas temperature lies well above 1.5 keV within all annuli. For each annulus counts-weighted response matrices were generated using the CIAO tasks MKWRMF and MKARF.

We fitted the background-subtracted spectrum with an APEC thermal plasma modified by Galactic absorption (6.4×10^{20} cm^{-2}, Dickey & Lockman 1990) to each annulus. The free parameters are temperature, iron abundance, and normalization (emission measure). (The fitted abundance is technically a metallicity since we fit the iron abundance as a free parameter and the abundances of all the other elements tied to iron in their solar ratios. However, iron dominates the metallicity.) The spectral fitting was performed with XSPEC (11.3.1i, Arnaud 1996) using the χ^2 minimization method. Hence, we rebinned all spectral channels to have a minimum of 20 counts per energy bin (necessary for the validity of the χ^2 method) and a signal-to-noise ratio of at least 3. The solar abundances in XSPEC are taken to be those given by Grevesse & Sauval (1998) which use the correct "new" photospheric value for iron which agrees also with the value obtained from solar-system meteorites (e.g., McWilliam 1997). To estimate the statistical errors on the fitted parameters we simulated spectra for each annulus using the best-fitting models and fit the simulated spectra in exactly the same manner as done for the actual data. From 100 Monte Carlo simulations we compute the standard deviation for each free parameter which we quote as the "1σ" error. (We note that these 1σ error estimates generally agree very well with those obtained using the standard $\Delta\chi^2$ approach in XSPEC.) All quoted errors are 1σ unless stated otherwise.

The radial profiles of temperature and iron abundance are shown in Figure 2; Table 1 gives the parameters obtained from the spectral fits for the centroid case; Figure 3 shows the ACIS-I spectra of two representative annuli and the associated best-fitting one-temperature model. The simple one-temperature model provides a good description of the spectral data in all annuli. For $R \gtrsim 75$ kpc the spectral fits for both the centroid and peak case agree very well. Over this region the temperature is consistent with a constant value ~ 8 keV as found also by previous studies of A644 with *ASCA* (e.g., White 2000; Bauer & Sarazin 2000). In contrast to these previous *ASCA* studies, the *Chandra* data clearly reveal that the iron abundance declines with radius from a value of $\sim 0.8 Z_\odot$ at $R \sim 75$ kpc to $\sim 0.25 Z_\odot$ at $R \sim 400$ kpc. Previous *ASCA* studies of A644 were consistent with a constant iron abundance profile (e.g., White 2000; Bauer & Sarazin 2000) within the large errors. We note also that the average iron abundance from *ASCA* ($\approx 0.5 Z_\odot$, scaled to our solar reference) obtained

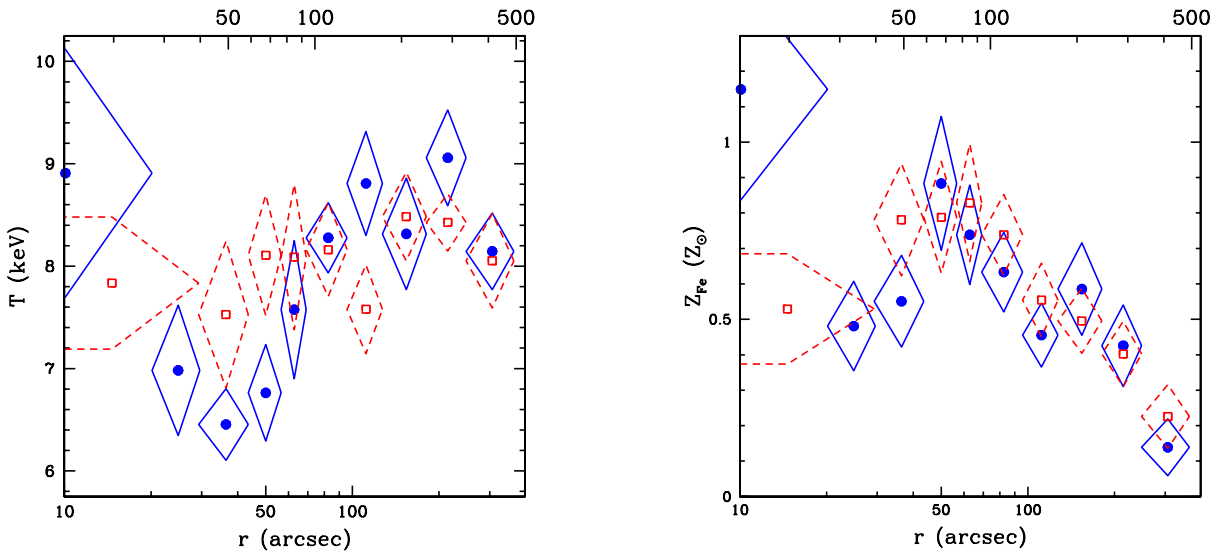

FIG. 2.— (*Left*) Radial temperature and (*Right*) metallicity profiles computed within circular annuli oriented about two different center positions: peak (circles: blue) and centroid (squares: red), as explained in the text. The top axis indicates radial units in kpc. The centroid results are also presented in Table 1.

TABLE 1
PARAMETERS FROM THE SPECTRAL FITS

Annulus	$R_{\rm in}$ (arcsec)	$R_{\rm in}$ (kpc)	$R_{\rm out}$ (arcsec)	$R_{\rm out}$ (kpc)	T (keV)	$Z_{\rm Fe}$ (solar)	$norm$ (10^{-3} cm^{-5})	(χ^2/dof)
1	0.0	0.0	29.3	39.3	7.8 ± 0.7	0.53 ± 0.16	2.54 ± 0.07	127.8/140
2	29.3	39.3	43.5	58.5	7.5 ± 0.7	0.78 ± 0.16	2.63 ± 0.06	118.3/146
3	43.5	58.5	56.6	76.0	8.1 ± 0.6	0.79 ± 0.16	2.86 ± 0.09	159.2/159
4	56.6	76.0	69.1	92.9	8.1 ± 0.7	0.83 ± 0.17	2.94 ± 0.10	168.6/165
5	69.1	92.9	95.9	128.9	8.2 ± 0.5	0.74 ± 0.12	6.23 ± 0.13	262.7/249
6	95.9	128.9	127.2	170.9	7.6 ± 0.4	0.55 ± 0.11	6.01 ± 0.12	235.9/225
7	127.2	170.9	180.8	242.9	8.5 ± 0.4	0.45 ± 0.09	7.92 ± 0.16	245.9/265
8	180.8	242.9	248.2	333.5	8.4 ± 0.3	0.40 ± 0.09	6.78 ± 0.15	254.4/248
9	248.2	333.5	364.1	489.2	8.1 ± 0.5	0.23 ± 0.09	6.65 ± 0.10	217.6/229

NOTE. — Results of fitting a single APEC plasma emission model modified by Galactic absorption directly to the annular spectra (i.e., without spectral deprojection) over 1.5-7 keV for the centroid case. The *norm* parameter is the emission measure of the APEC model as defined in XSPEC: $10^{-14}(\int n_e n_p dV)/4\pi D^2(1+z)^2$ with units cm^{-5}. The quoted errors are 1σ computed using the Monte Carlo procedure described in §4.

by White (2000) agrees well with our *Chandra* results.

For $R \gtrsim 75$ kpc the declining radial profile of iron abundance, approximately isothermal gas profile, and regular image morphology are very characteristic of relaxed "cool core" clusters (e.g., Molendi & Pizzolato 2001; De Grandi et al. 2004). Inspection of Figure 2 reveals that the region $R \lesssim 75$ kpc is more complex. The iron abundance profile is approximately constant for the centroid case, with marginal evidence for a central dip. In the peak case, the profile declines and then appears to increase in the central bin: the value in the central bin (1.15 ± 0.31 solar) is inconsistent with that in the adjacent bin at the $\approx 2.5\sigma$ level.

The temperature profile for $R \lesssim 75$ kpc does not correspond to a typical cool-core cluster. In the centroid case, the temperature is consistent with isothermal. In the peak case, the temperature declines inward to $R \sim 50$ kpc like a cool-core cluster but then rises significantly in the central bin ($T = 8.9 \pm 1.2$ keV). The 99% confidence lower limit on the temperature estimated using $\Delta\chi^2 = 6.63$ is $T = 6.7$ keV, still larger than the minimum value of $T = 6.5$ keV reached near $R = 50$ kpc. A power law fit to the temperature profile of the inner three radial bins is inconsistent with a constant value at the 2.3σ level and is highly inconsistent with the declining temperature central profiles characteristic of cool core clusters.

Despite the good quality of the fits, we examined whether they could be improved further. Allowing abundances other than iron to vary separately did not yield noticeable improvement. Adding another temperature component also had no effect on the fits, even when energies down to 0.5 keV were included. Consequently, we found no need for an additional multiphase cooling flow component in the spectra. Previous *ASCA* studies were divided between indicating a massive cooling flow ($\gtrsim 60 M_\odot$ yr^{-1}, Bauer & Sarazin 2000) and no cooling flow ($\lesssim 40 M_\odot$ yr^{-1}, White 2000).

Using a standard model of a gas cooling at constant pressure as implemented in our previous studies (e.g., Buote et al. 2003a), our *Chandra* results indicate a best-fitting cooling rate of zero with 90% upper limits of

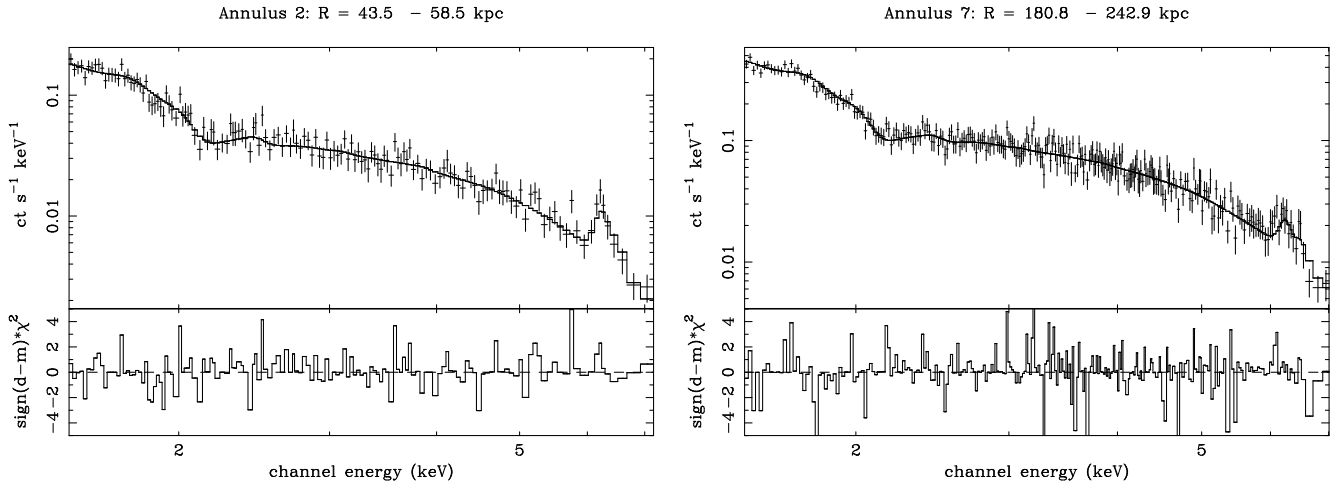

FIG. 3.— ACIS-I spectra accumulated within (*Left Panel*) annulus #2 and (*Right Panel*) annulus #7 for annuli located about the centroid (Table 1). Each spectrum is fitted with an APEC plasma model modified by Galactic absorption over 1.5-7 keV as discussed in §4.

$\approx 5\ M_\odot\ \mathrm{yr}^{-1}$ in all annuli except annulus 1 (referring to the centroid case), where $\dot{M} = 7(< 11)\ M_\odot\ \mathrm{yr}^{-1}$ (90% confidence). (We note that sometimes evidence for a cooling flow and multiphase gas in clusters has been claimed based on the analysis of CCD spectra extracted from a large aperture covering, e.g., the entire putative cooling flow region (e.g., Clarke & et al. 2004). However, the distribution of temperatures produced by the radial variation of a single-phase medium within the putative cooling flow aperture, as well as that contributed by the projection of higher temperature gas outside the aperture if the data are not deprojected, generally cannot be distinguished from a two-temperature medium or a cooling flow (e.g., Buote 1999; Buote et al. 2003a). Hence, we have explored the need for multiphase gas using the narrowest annuli allowed by the data quality.)

Although the hardness ratio map displayed no significant azimuthal variations (§3), we searched for azimuthal spectral variation by dividing up the annuli into four equal sectors We rebinned the radial bins by a factor of two to achieve enough signal for interesting constraints. When fitting a single APEC component to each sector we found no evidence for azimuthal spectral variations, consistent with the findings from the hardness ratio map. The temperatures and iron abundances in each sector within an annulus were found to be consistent within their $\approx 90\%$ confidence limits. In particular, we do not find the > 15 keV temperature spike in a region a few arcminutes to the East of the center reported by Bauer & Sarazin (2000) from *ASCA*. (The orientations of our sectors were oriented approximately to match those of sectors 2-5 of Bauer & Sarazin 2000.)

Finally, we have studied the sensitivity of the results to various sources of systematic error which we summarize below:

Deprojection: We performed a non-parametric deprojection using the "onion-peeling" method as implemented in our previous studies (e.g., Buote 2000; Buote et al. 2003a; Lewis et al. 2003). That is, one begins by determining the spectral model in the bounding annulus and then works inward by subtracting off the spectral contributions from the outer annuli. This technique tends to introduce fluctuations between parameters in adjacent radial bins. We found that to obtain results of comparable quality to the projected analysis it was necessary either to fix the temperature at a constant value near 8 keV or restrict the radial variation in the the iron abundance so that its logarithmic slope was $\lesssim \pm 1$. After imposing either of these restrictions we obtain results consistent with those reported above for the projected analysis – both in terms of fit quality and parameter values. (We note that these results for the temperatures and iron abundances obtained using our implementation of the "onion-peeling" method are very consistent with those obtained using the deprojection scheme provided in XSPEC using the PROJCT routine and require the same restrictions on the temperatures and iron abundances noted above.)

Galactic Column Density and Bandwidth: When energies below ~ 1 keV are included in the fits then a model assuming the nominal foreground Galactic column density ($6.4 \times 10^{20}\ \mathrm{cm}^{-2}$) overestimates the flux at low energies, especially near 0.5-0.6 keV. If N_H is allowed to vary the fits are improved substantially within each annulus; e.g., in annulus 4 $\Delta\chi^2 = 45.9$ for 228 dof. The best-fitting column densities are $\approx 14 \times 10^{20}\ \mathrm{cm}^{-2}$– about twice the Galactic value. Since the excess column densities apparently do not vary with radius it is likely that the excess is associated with an underestimate of the Galactic column. (Using the background models described below we verified that the inferred excess column density is not the result of over-subtracting the soft background using the standard templates of nominally blank fields.) Our result is similar to that reported by an *XMM* study of A478 (Pointecouteau et al. 2004).

Compared to the results presented above for energies above 1.5 keV, the temperature and iron abundance are mostly unaffected when fitting down to 0.5 keV with a column density about twice the Galactic value. The most significant change is a systematic decrease of ≈ 0.7 keV in the temperature values in all annuli, but the shape of the radial temperature profile is preserved. Although we expect the excess column density is of Galactic origin we preferred to confine our analysis to energies above

1.5 keV to avoid sensitivity to the precise value.

Background: As described in §2, for comparison to results obtained using the standard blank background fields we also constructed a model background by fitting the total (source plus background) spectrum of regions of the ACIS-I as far away from the center of A644 as possible. We found that results obtained using this modeled background agreed extremely well with those of the standard blank fields. As expected, by far the largest differences were observed in annulus 9; e.g., $T = 8.6 \pm 0.6$ keV using the modeled background compared to $T = 8.1 \pm 0.5$ keV for the standard blank fields.

Plasma Code: We investigated the sensitivity of our results to the plasma code using the MEKAL model. The quality of the fits and the temperature values were found to be very consistent within the 1σ errors. The iron abundance values also were consistent with those obtained using the APEC code, though the values obtained with the MEKAL code were generally smaller by 10%-20%. These results are consistent with previous studies (Buote et al. 2003a,b; Humphrey et al. 2004).

Calibration: We explored the sensitivity of our results to the version of the *Chandra* calibration using previous versions of CIAO (v3.0.2) and the CALDB (v2.26). We found the results on the fitted spectral parameters to be consistent with those quoted above within the estimated $\approx 1\sigma$ statistical errors.

5. GRAVITATING MASS AND GAS FRACTION

To determine the gravitating mass distribution from X-ray observations requires the hot gas to be in hydrostatic equilibrium. Both N-Body simulations and gravitational lensing studies confirm the reliability of X-ray mass measurements, particularly for clusters with regular X-ray image morphologies (e.g., for a review see Buote 2004). The assumption of hydrostatic equilibrium should be valid outside the central $\sim$ 75 kpc region of A644. Outside the core region the derived radial variations in the density and temperature of the hot gas agree for both the cases where the cluster center is defined as the surface brightness peak or centroid. Consequently, we exclude the central three annuli (defined in Table 1) from our default analysis, though for comparison we summarize results obtained using all annuli.

The approach we use to calculate the gravitating mass distribution follows closely our previous studies (Lewis et al. 2003; Buote & Lewis 2004). As is standard we assume spherical symmetry to provide a spherically averaged mass profile appropriate for comparison to other observations and to the spherically averaged mass profiles obtained from cosmological simulations. In the equation of hydrostatic equilibrium we evaluate the derivatives of the three-dimensional gas density ($\rho_{\rm g}$) and temperature (T) using simple parameterized models as discussed below.

For our default analysis we projected parameterized models of the three-dimensional quantities, $\rho_{\rm g}$ and T, and fitted these projected models to the results obtained from our analysis of the data projected on the sky (Table 1). In this manner we obtained good constraints on the three-dimensional radial profiles of $\rho_{\rm g}$ and T. Although our analysis closely follows our previous studies, we note two minor improvements. First, when fitting models to the radial profiles of the gas density and temperature to the data binned in annuli on the sky (as given in Table 1) we integrated the models over each radial bin (rather than only evaluating at a single point within the bin) to provide a consistent comparison. Second, when projecting models of the gas density and temperature along the line of sight we also included the radial variation in the plasma emissivity ($\Lambda(T, Z_{\rm Fe})$).

In Figure 4 we show the radial profile of the emission-weighted projection of ${\rho_{\rm g}}^2$; i.e., the "norm" parameter (see caption to Table 1) of the APEC model divided by the area of the annulus. A single β model provides a good description of the data with fit residuals $\leq 5\%$ (Table 2). Because the inner three annuli were excluded, a marginally larger value of β was obtained compared to the surface brightness fits (§3). Adding a second β-model component provides small improvement in the fits with smaller residuals ($\leq 3\%$) than the 1β model (Table 2); the 2β model is displayed in Figure 4. Although the parameters for the 2β model are not as well constrained as those for the 1β model we adopt the 2β model for our analysis of the mass distribution because it describes the data a little better. Note that if the inner three annuli are included then the parameters obtained are consistent with those in Table 2 but are somewhat better constrained. For the case where the annuli are oriented about the emission peak the second component of a 2β model (fitted to all annuli) matches very well the 1β-model results obtained for the centroided case listed in Table 2, demonstrating the similarity of the gas density profiles obtained outside the core region for the peak and centroid case.

The radial profile of the emission-weighted projection of T is shown in Figure 4 (middle panel) along with the best-fitting power-law fit. The simple power law is an excellent fit (Table 2) and demonstrates that the temperature profile is consistent with isothermal within the estimated 1σ errors. Notice that despite the inner three annuli being excluded from the fits the model describes those data points well.

We constructed the mass profile using the models just described for the gas density and temperature. Following previous studies (e.g., Lewis et al. 2003), for each annulus listed in Table 2 we assign a single (three-dimensional) radius value, $r \equiv [(R_{\rm out}^{3/2} + R_{\rm in}^{3/2})/2]^{2/3}$, where $R_{\rm in}$ and $R_{\rm out}$ are respectively the inner and outer radii of the (two-dimensional) annulus. The radial mass profile is plotted in Figure 4 using the 2β-model for $\rho_{\rm g}$ and the power law model for T. (We emphasize that although the mass values for the inner three data points are shown, being derived from the gas density and temperature models, they are not included in the fits.)

The NFW model is a good smooth fit when excluding the inner three radial bins (Figure 4). We obtain $\chi^2 = 6.9$ for 4 dof with fit residuals $\leq 15\%$. Because the mass data points are correlated it is necessary to recalibrate the χ^2 statistic to examine goodness of fit using our Monte Carlo simulations (§4); i.e., for each set of parameters for the gas density and temperature profiles obtained for each simulation, a mass profile is constructed and then fitted with an NFW model. These simulations indicate the the χ^2 value quoted above is within one standard deviation of the expected value.

In Table 3 we give the parameters of the NFW fit and

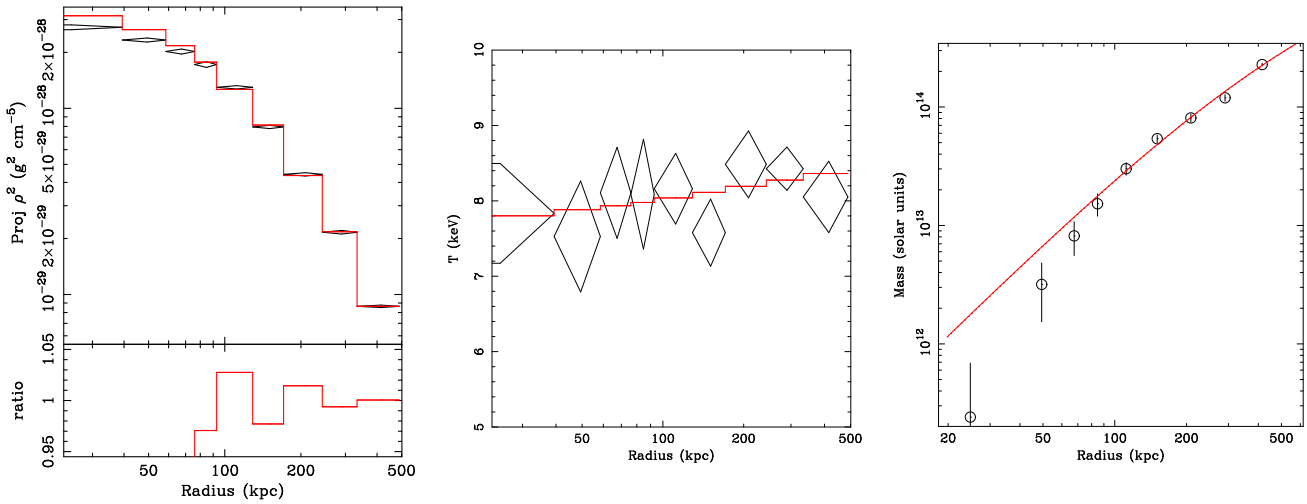

FIG. 4.— Models fitted to radial profiles (centroid case) as discussed in §5. In each case the inner three data points are excluded from the fits. (*Left*) *Chandra* radial profile of the projected gas density squared ($\int \rho_{\rm g}{}^2 \Lambda(T, Z_{\rm Fe}) dl / \Lambda_{\rm ann}$) obtained by dividing the *norm* parameter of the APEC model (Table 1) by the area of the annulus; $\Lambda_{\rm ann}$ is the plasma emissivity evaluated using T and $Z_{\rm Fe}$ of the annulus. The diamonds represent the binned data and the solid line the best-fitting double-beta model. The fit residuals are plotted in the lower panel. (*Center*) Temperature profile of the binned data (diamonds) and best-fitting power-law model. (*Right*) Mass profile (circles and error bars) and best-fitting NFW model.

TABLE 2
DEPROJECTED RADIAL PROFILES OF GAS DENSITY AND TEMPERATURE

Gas Density							
Model	$(\chi^2/{\rm dof})$	r_c (kpc)	β	$\rho_{\rm g_0}$ (10^{-26} g cm^{-3})	$r_{c,2}$ (kpc)	β_2	$\rho_{\rm g_{0,2}}$ (10^{-26} g cm^{-3})
1β	12.1/3	120 ± 8	0.64 ± 0.02	2.27 ± 0.12			
2β	4.3/0	213 ± 33	2.0 ± 0.3	2.19 ± 0.24	352 ± 115	1.1 ± 0.3	0.82 ± 0.17

Temperature			
Model	$(\chi^2/{\rm dof})$	T_{100} (keV)	p
power law	2.7/4	7.9 ± 0.4	0.04 ± 0.05

NOTE. — These models were (emission-weighted) projected along the line of sight and fitted to the data about the centroid excluding the inner three annuli. T_{100} is the temperature evaluated at $r = 100$ kpc and p is the exponent. Note that the best-fitting value of β for the 2β model was not well constrained and pegged at the upper limit we allowed in the fits.

the estimated statistical and systematic errors. The estimates for the systematic errors are mostly based on our discussion in §4, and we have also included the differences obtained when using a 1β model to parameterize the $\rho_{\rm g}$ profile. (Note we do not provide an estimated error arising from the deprojection method because the statistical errors are considerably larger when using the onion-peeling method.) The derived concentration parameter (≈ 6) and virial radius (≈ 2.9 Mpc) imply a virial mass of $\approx 1.5 \times 10^{15} M_\odot$ appropriate for a massive galaxy cluster. The value of c is consistent with that expected from CDM (e.g., Thomas et al. 2001; Tasitsiomi et al. 2004).

We mention that within the central region (i.e., the central three annuli), where the assumption of hydrostatic equilibrium is suspect, the mass density profile is flatter than NFW; i.e., the cumulative mass profile at small radii lies below NFW as seen in Figure 4. However, for the case where the annuli are centered about the emission peak we find the mass profile within the central ~ 70 kpc is highly uncertain but consistent with NFW. (To obtain a reasonable smooth fit to the centrally peaked temperature profile in this case, we modeled the profile with two power laws with exponential cut-offs at both ends.) The smaller mass values in the core for the centroid case are attributed to the flatter density and temperature profiles obtained with respect to the peak case; i.e., when the annuli are not positioned about the emission peak radial differences in spectral quantities are smeared out.

6. CONCLUSIONS

Outside the core ($R \sim 75$ kpc $\sim 0.03 r_{\rm vir}$) the hot ICM has properties consistent with a (relaxed) cool-core cluster out to the largest radii investigated ($R \sim 415$ kpc $\sim 0.14 r_{\rm vir}$). The X-ray surface brightness is very regular, moderately elliptical in shape, with no evidence of sub-

TABLE 3
PARAMETERS OF NFW FIT TO THE GRAVITATING MATTER PROFILE

	Best	ΔStatistical	ΔBackground	ΔPlasma	ΔBandwidth	ΔCalibration	$\Delta\rho_g$
c	6.1	±1.2	-0.4	$+1.2$	-0.4	$+0.1$	$+0.4$
$r_{\rm vir}$(Mpc)	2.9	±0.4	$+0.3$	-0.3	-0.2	-0.1	-0.1

NOTE. — The virial radius ($r_{\rm vir}$) is defined to be the radius where the enclosed average mass density equals $103\rho_c(z)$ appropriate for the ΛCDM concordance cosmology (e.g., Eke et al. 1998). The inner three annuli are excluded from the fits. The "Best" column indicates the best-fitting value and "ΔStatistical" the 1σ statistical error. The other columns refer to systematic differences in the best-fitting values obtained for different choices (see end of §4) in the background, plasma code, bandwidth, and calibration. For the bandwidth case the data are fitted down to 0.5 keV using a fixed foreground column density of 14×10^{20} cm^{-2}(see end of §4). The final column refers to differences obtained when using a 1β model to parameterize the gas density.

structure; previous *ROSAT* studies generally indicated a relaxed cluster on such scales (e.g., Buote & Tsai 1996). The radial profile of the density of the ICM is fitted well with a single β model, with a double β model providing slight improvement. The temperature profile is consistent with isothermal or gently rising (e.g., Allen et al. 2001; Vikhlinin & et al. 2004). The entropy factor ($S\equiv k_BT/n_e^{2/3}$, e.g., $S=797\pm21$ keV cm^2 at $R=0.14r_{\rm vir}$) is consistent with those observed in cool-core clusters (e.g., Piffaretti & et al. 2004). The iron abundance declines with increasing radius (e.g., De Grandi et al. 2004). The gravitating mass profile is well fitted by an NFW profile with reasonable concentration parameter for a halo of its virial mass. Finally, the gas fraction (0.076 ± 0.002 at $R=0.14r_{\rm vir}$) is quite typical of relaxed clusters observed by *Chandra* and produced in CDM simulations (e.g., Allen et al. 2004).

Inside the core, however, the *Chandra* data reveal an irregular, disturbed system. The X-ray image displays asymmetrical isophotes about the emission peak which are offset from the global emission centroid by ≈ 50 kpc. When oriented about the emission peak, the temperature profile of the ICM declines towards the center (down to $R\sim50$ kpc), very much resembling a cool-core cluster. But at small radii the temperature profile turns around and increases toward the center; i.e., the inner temperature profile is inconsistent with a constant at the 2.3σ level. Both the iron abundances and entropy profiles mirror the shape of the temperature profile with an excess at the center.

Since A644 does not possess significant radio emission (Burns 1990), and the *Chandra* image does not show any X-ray cavities, the suppression of a cooling flow cannot be attributed to the present day feedback from an AGN. Nor is it easily ascribed to heating by a past radio outburst from the black hole in the cD, because the synchrotron lifetime of 1 GHz-emitting cosmic rays is $\sim10^8$ yr for a magnetic field strength of a few μGauss in the cluster ICM. Since this energy loss timescale is comparable to the sound-crossing time for the cluster core (and thus to the time needed to heat the core), the core should remain hot for about the same time as the 1 GHz radio emission remains visible after heating is terminated. It is even more difficult to explain heating of the "hot spot" (i.e., the central "hot" radial bin oriented about the emission peak – see Figure 2) by an AGN in the recent past, because an even shorter time since the cessation of cosmic ray injection is required due to its smaller physical size.

Nevertheless, a search for a steep-spectrum radio source would be worthwhile. The absence of low-frequency radio emission (e.g., VLA Low-frequency Sky Survey; Cohen et al. 2004) would be an even more powerful test against the AGN heating model in A644, because 100 MHz-emitting cosmic rays have three times longer lifetimes in comparable magnetic fields. Moreover, although the higher temperature in the "hot spot" appears to be accompanied by a sharp increase in iron abundance, supernovae are a most unlikely heating source for even this small portion of the core because the required number of supernovae would need to be accompanied by a recent, galaxy-sized ($\geq10^9M_\odot$) starburst. Neither a blue galaxy nor a luminous emission-line nebula are visible in the cluster core of A644 (Hu et al. 1985).

However, the morphological irregularities in the core of the X-ray image are very likely the result of merging. The cD galaxy (2MASX J08172559 -0730455) is located ≈20 kpc South of the X-ray emission peak nearly along the direction of the centroid shift noted in §3. It is also ≈40 kpc displaced from the centroid of the X-ray emission computed from larger radii. Evidently the cD galaxy and core ICM are "sloshing" in the potential well of the main cluster, and this energy has prevented the establishment of a cooling flow. The metallicity peak measured within the innermost radial bin probably indicates that previous merging did not destroy the initial peak, created when it was spatially coincident with the cD galaxy. This is because, as argued above, the peak is unlikely the result of very recent supernova enrichment. Also, the visual appearance of the A644 galaxies is quite diffuse, stretching ~2 Mpc linearly across the sky, suggesting a system far from relaxation. This morphology strengthens the argument for an on-going merger.

The properties of A644 (this paper), A2029 (Lewis et al. 2002, 2003), and A2589 (Buote & Lewis 2004) have important similarities. Their X-ray images indicate a peak which is offset from the centroid of the global X-ray halo, with A644 displaying the most extreme shift (≈60 kpc offset) compared to the others (A2589: ≈10 kpc, A2029: ≈4 kpc). Other than these offsets, the X-ray emission is very regular in each case with no indications of cavities as are seen in cool-core clusters with AGN. [4] Two of these clusters

[4] We remark that Clarke & et al. (2004) have emphasized the existence of low-level ($\approx10\%$) surface brightness deviations from a smooth elliptical model in the central ~10 kpc of A2029 using the AO-1 *Chandra* image, and claim that the WAT morphology

have no detected AGN radio emission, while A2029 has a WAT morphology AGN, very unusual (unique to our knowledge) for a cool-core cluster. Finally, the lack of nebular emission lines in the cD galaxies are characteristic of non-cool-core clusters (Cardiel et al. 1998).

Of these three clusters only A644 possesses a central temperature peak. Although A644 appears to be unique in that its temperature profile declines toward the center and then rises, there are a few reports of clusters in the literature with temperature profiles measured by either *Chandra* or *XMM* that peak at their centers. The clusters A2218 (Govoni et al. 2004; Pratt & et al. 2005) and A3921 (Belsole et al. 2005) are violent, advanced mergers with with pronounced asymmetrical surface brightness and temperature distributions uncharacteristic of A644, A2029, and A2589. Another cluster with a reported central temperature peak is A401 (Sakelliou & Ponman 2004), which is in the early stages of a major merger (with A399). Nevertheless, Sakelliou & Ponman (2004) argue that the properties of A401 are determined primarily from its own hierarchical formation before interaction with A399. In this context it is interesting that A401 has a weak radio halo since we have suggested that radio halos form only in massive clusters where a violent merger has proceeded fully into the cluster core (Buote 2001). If the other clusters had a similar history, their lack of radio halos indicate they are presently at much more evolved states than A401.

anitcorrelates with these small fluctuations. Using a more recent, deeper (80 ks) Chandra exposure we confirm $\approx 10\%$ deviations in the surface brightness (Zappacosta et al. 2005, in prep), but we do not confirm a strong anticorrelation with the WAT morphology as seen in other cool-core clusters. Compared to other cool-core clusters with obvious central disturbances these $\approx 10\%$ deviations in the surface brightness, which translate to even smaller ($\approx 5\%$) deviations in the gas density, indicate that the core of A2029 is in a much more relaxed state. For comparison, we find that Perseus, a cool-core cluster with an obvious distrurbance in the core, displays up to 50% fluctuations in the surface brightness. It should be added that, unlike A2029, Perseus also has strong azimuthal fluctuations in the temperature and metallicity which, however, apparently consipire to produce approximate azimuthal balance in the gas pressure and therefore approximate hydrostatic equilibrium (Sanders et al. 2004).

In the paradigm wherein the energy output from an AGN disrupts cooling flows, it is expected that just prior to the onset of AGN feedback a cluster will have the characteristics of a cool-core cluster but without significant radio emission or X-ray cavities. Indeed, the clusters A644, A2029, and A2589 are excellent candidates for this pre-feedback state, with A644 being at a relatively early state and A2029 at the very latest evolutionary state, where an AGN outburst has already occurred but little or no heating from AGN-generated cosmic rays has commenced. The extremely advanced evolutionary states of A2029 and A2589 make them ideal for studies of their core mass profiles using the assumption of hydrostatic equilibrium.

We thank A. Lewis for his participation in this project at early stages. J.T.S. thanks A. Venketasen for useful discussions of cluster heating mechanisms. D.A.B. acknowledges partial support from NASA under grant NAG5-13059 issued through the Office of Space Science Astrophysics Data Program. Partial support for this work was also provided by the National Aeronautics and Space Administration through Chandra Award Number GO1-2130X issued by the Chandra X-ray Observatory Center, which is operated by the Smithsonian Astrophysical Observatory for and on behalf of the National Aeronautics and Space Administration under contract NAS8-03060.

REFERENCES

Allen, S. W., Schmidt, R. W., Ebeling, H., Fabian, A. C., & van Speybroeck, L. 2004, MNRAS, 258
Allen, S. W., Schmidt, R. W., & Fabian, A. C. 2001, MNRAS, 328, L37
Arnaud, K. A. 1996, in ASP Conf. Ser. 101: Astronomical Data Analysis Software and Systems V, Vol. 5, 17
Bîrzan, L., Rafferty, D. A., McNamara, B. R., Wise, M. W., & Nulsen, P. E. J. 2004, ApJ, 607, 800
Böhringer, H., Matsushita, K., Churazov, E., Finoguenov, A., & Ikebe, Y. 2004, A&A, 416, L21
Bauer, F. & Sarazin, C. L. 2000, ApJ, 530, 222
Belsole, E., Sauvageot, J.-L., Pratt, G. W., & Bourdin, H. 2005, A&A, 430, 385
Blanton, E. L., Sarazin, C. L., McNamara, B. R., & Wise, M. W. 2001, ApJ, 558, L15
Buote, D. A. 1999, MNRAS, 309, 685
—. 2000, ApJ, 539, 172
—. 2001, ApJ, 553, L15
Buote, D. A. 2004, in IAU Symp. 220: Dark Matter in Galaxies, 149
Buote, D. A., Brighenti, F., & Mathews, W. G. 2004, ApJ, 607, L91
Buote, D. A. & Canizares, C. R. 1994, ApJ, 427, 86
Buote, D. A., Jeltema, T. E., Canizares, C. R., & Garmire, G. P. 2002, ApJ, 577, 183
Buote, D. A. & Lewis, A. D. 2004, ApJ, 604, 116
Buote, D. A., Lewis, A. D., Brighenti, F., & Mathews, W. G. 2003a, ApJ, 594, 741
—. 2003b, ApJ, 595, 151
Buote, D. A. & Tsai, J. C. 1996, ApJ, 458, 27
Burns, J. O. 1990, AJ, 99, 14
Burns, J. O., Loken, C., Roettiger, K., Rizza, E., Bryan, G., Norman, M. L., Gómez, P., & Owen, F. N. 2002, New Astronomy Review, 46, 135
Cardiel, N., Gorgas, J., & Aragon-Salamanca, A. 1998, MNRAS, 298, 977
Carter, D. & Metcalfe, N. 1980, MNRAS, 191, 325
Clarke, T. E. & et al. 2004, astro-ph/0408068
Cohen, A. S., Lane, W. M., Kassim, N. E., Lazio, T. J. W., Cotton, W. D., Perley, R. A., Condon, J. J., & Erickson, W. C. 2004, American Astronomical Society Meeting Abstracts, 205,
David, L. P., Nulsen, P. E. J., McNamara, B. R., Forman, W., Jones, C., Ponman, T., Robertson, B., & Wise, M. 2001, ApJ, 557, 546
De Grandi, S., Ettori, S., Longhetti, M., & Molendi, S. 2004, A&A, 419, 7
Dickey, J. M. & Lockman, F. J. 1990, ARA&A, 28, 215
Edge, A. C., Stewart, G. C., & Fabian, A. C. 1992, MNRAS, 258, 177
Eilek, J. A., Burns, J. O., Odea, C. P., & Owen, F. N. 1984, ApJ, 278, 37
Eke, V. R., Navarro, J. F., & Frenk, C. S. 1998, ApJ, 503, 569
Ettori, S. & Fabian, A. C. 1999, MNRAS, 305, 834
Ettori, S., Fabian, A. C., Allen, S. W., & Johnstone, R. M. 2002, MNRAS, 331, 635
Fabian, A. C. 2004, astro-ph/0407484
Fabian, A. C., Sanders, J. S., Ettori, S., Taylor, G. B., Allen, S. W., Crawford, C. S., Iwasawa, K., Johnstone, R. M., & Ogle, P. M. 2000, MNRAS, 318, L65
Fujita, Y., Suzuki, T. K., & Wada, K. 2004, ApJ, 600, 650

Govoni, F., Markevitch, M., Vikhlinin, A., VanSpeybroeck, L., Feretti, L., & Giovannini, G. 2004, ApJ, 605, 695
Grevesse, N. & Sauval, A. J. 1998, Space Science Reviews, 85, 161
Hu, E. M., Cowie, L. L., & Wang, Z. 1985, ApJS, 59, 447
Humphrey, P. J., Buote, D. A., & Canizares, C. R. 2004, ApJ, 617, 1047
Lewis, A. D., Buote, D. A., & Stocke, J. T. 2003, ApJ, 586, 135
Lewis, A. D., Stocke, J. T., & Buote, D. A. 2002, ApJ, 573, L13
Loken, C., Roettiger, K., Burns, J. O., & Norman, M. 1995, ApJ, 445, 80
Mathews, W. G. & Brighenti, F. 2003, ARA&A, 41, 191
Mazzotta, P., Edge, A. C., & Markevitch, M. 2003, ApJ, 596, 190
McNamara, B. R., Wise, M., Nulsen, P. E. J., David, L. P., Sarazin, C. L., Bautz, M., Markevitch, M., Vikhlinin, A., Forman, W. R., Jones, C., & Harris, D. E. 2000, ApJ, 534, L135
McWilliam, A. 1997, ARA&A, 35, 503
Molendi, S. & Pizzolato, F. 2001, ApJ, 560, 194
Norman, M. L. & Bryan, G. L. 1999, Lecture Notes in Physics, Berlin Springer Verlag, 530, 106
Owen, F. N., Burns, J. O., & White, R. A. 1984, in ASSL Vol. 111: Clusters and Groups of Galaxies, 295
Peres, C. B., Fabian, A. C., Edge, A. C., Allen, S. W., Johnstone, R. M., & White, D. A. 1998, MNRAS, 298, 416
Peterson, J. R., Kahn, S. M., Paerels, F. B. S., Kaastra, J. S., Tamura, T., Bleeker, J. A. M., Ferrigno, C., & Jernigan, J. G. 2003, ApJ, 590, 207
Peterson, J. R., Paerels, F. B. S., Kaastra, J. S., Arnaud, M., Reiprich, T. H., Fabian, A. C., Mushotzky, R. F., Jernigan, J. G., & Sakelliou, I. 2001, A&A, 365, L104
Piffaretti, r. & et al. 2004, astro-ph/0412233
Pointecouteau, E., Arnaud, M., Kaastra, J., & de Plaa, J. 2004, A&A, 423, 33
Pratt, G. w. & et al. 2005, astro-ph/0502322
Roettiger, K., Burns, J. O., & Loken, C. 1996, ApJ, 473, 651
Sakelliou, I. & Ponman, T. J. 2004, MNRAS, 351, 1439
Sanders, J. S., Fabian, A. C., Allen, S. W., & Schmidt, R. W. 2004, MNRAS, 349, 952
Tamura, T., Kaastra, J. S., Peterson, J. R., Paerels, F. B. S., Mittaz, J. P. D., Trudolyubov, S. P., Stewart, G., Fabian, A. C., Mushotzky, R. F., Lumb, D. H., & Ikebe, Y. 2001, A&A, 365, L87
Tasitsiomi, A., Kravtsov, A. V., Gottlöber, S., & Klypin, A. A. 2004, ApJ, 607, 125
Thomas, P. A., Muanwong, O., Pearce, F. R., Couchman, H. M. P., Edge, A. C., Jenkins, A., & Onuora, L. 2001, MNRAS, 324, 450
Vikhlinin, A. & et al. 2004, astro-ph/0412306
White, D. A. 2000, MNRAS, 312, 663
Xu, H., Kahn, S. M., Peterson, J. R., Behar, E., Paerels, F. B. S., Mushotzky, R. F., Jernigan, J. G., Brinkman, A. C., & Makishima, K. 2002, ApJ, 579, 600